Structural and Optical Characterization of As-grown and Annealed $Zn_xCd_{1-x}S$ Thin-films by CBD for Solar Cell Applications

E.M.K. Ikball Ahamed*‡, N.K. Das*, A.K.S. Gupta*, M.N.I. Khan**, M.A. Matin*, N. Amin***

* Department of Electrical and Electronic Engineering, Chittagong University of Engineering and Technology, Chattogram-4349, Bangladesh

** Materials Science Division, Atomic Energy Centre, Dhaka

*** Institute of Sustainable Energy, Universiti Tenaga Nasional (@ The Energy University), Jalan IKRAM-UNITEN, 43000 Kajang, Selangor, Malaysia

(ikballahamed@cuet.ac.bd, nipudas@cuet.ac.bd, aksengupta@cuet.ac.bd, ni_khan77@yahoo.com, mamatin@cuet.ac.bd, nowshad@uniten.edu.my)

‡ Corresponding Author; E.M.K. Ikball Ahamed, Department of Electrical and Electronic Engineering, Chittagong University of Engineering and Technology, Chattogram-4349, Bangladesh, Tel: +8801737592825, ikballahamed@cuet.ac.bd

Received: 28.07.2020 Accepted:29.08.2020

Abstract- We report the synthesis of $Zn_xCd_{1-x}S$ (x=0 to 0.41) thin-films by chemical bath deposition technique and annealing of the as-grown $Zn_{0.31}Cd_{0.69}S$ films at 200°C, 350°C and 500°C. The structural properties, optical properties, surface morphology and elemental composition of the films are characterized by XRD, UV-Vis N.I.R. spectroscopy, EDX. and FESEM. The thickness of the as-grown films is measured by the DEKTAK stylus profilometer and is in the range of ~100 nm-120 nm. The as-grown films show quasi-crystalline nature with preferential orientation along (002) hexagonal plane and the crystallinity is declined with the increment of zinc content. Also, the FESEM micrographs show the homogeneous growth, pinhole-free surface and compactness of the films. The transmission edge is shifted towards the short wavelength region as the relative zinc content increases, which confirms the significant reduction of photon absorption in the blue region of the solar spectrum. The as-grown films show average transmittance of ~80-90% along with a tunable bandgap of 2.50eV to 3.35eV for the variation of relative zinc content from 0 to 0.41. The annealing treatment improves the crystalline properties of $Zn_{0.31}Cd_{0.69}S$ film and the best crystallinity is obtained at 350°C temperature. Meanwhile, the annealed $Zn_{0.31}Cd_{0.69}S$ films also exhibit a variable bandgap of 2.85eV, 3.10eV and 3.22eV at 200°C, 350°C and 500°C respectively whereas the bandgap of the as-grown film is 3.12eV. Annealed $Zn_{0.31}Cd_{0.69}S$ thin-film at 350°C having enhanced structural properties without affecting optical characteristics and therefore it can be suitable as a good alternative buffer layer for thin-film solar cell applications.

Keywords- Thin-film, Chemical bath deposition, $Zn_xCd_{1-x}S$, Annealing, XRD, UV-Vis NIR, FESEM

1. Introduction

Solar photovoltaic is the effective way to convert sunlight directly into electricity and represents a major alternative to conventional fossil fules [1]. Thin-film solar cells are second-generation solar cells that utilize direct bandgap materials and provide the advantage of less material consumption [2]. Cadmium Sulfide (CdS) is a group II-VI compound semiconductor material that is used as a common n-type hetero partner as well as a buffer layer for thin-film solar cell applications [3]. As the bandgap of the CdS buffer layer is 2.42eV, it absorbs higher energy photons especially in the blue region of the solar spectrum which does not contribute to photo-generated current in a solar cell [4-6]. The Photocurrent losses can be compensated by the deposition of a very thin CdS layer. But thinning the CdS results in a severe degradation in cell performance in the practical situation by creating shunting effect and excess pinhole formation in hetero-interface, which drastically reduces the open-circuit voltage *(V_{oc})* and fill factor (FF). Also, considering the environmental and hazardous impact of cadmium, researchers concentrate on cadmium-free buffer layers. In that case, depositing a relatively higher bandgap buffer layer can help to alleviate the problems associated with CdS thin-films. To enhance the optical property of the

buffer layer and the short circuit current density of the solar cell, utilization of an elective material based on zinc, e.g., ZnS, $Zn(O,S,OH)_x$, etc. having higher bandgap than CdS, has been suggested by many researchers [7, 8]. However, most of the researchers and manufacturers haven't been able to accomplish large scale manufacturing of ZnS based PV cells and modules expect Solar Frontier, Japan [9] due to the low repeatability and reproducibility of Zn based material [10]. A sulfide material $Zn_xCd_{1-x}S$ composed of Zn and Cd can be a promising alternative because of its higher bandgap than CdS and stable process parameters. $Zn_xCd_{1-x}S$ (here, $x= Zn/[Zn+Cd]$) is a ternary compound semiconductor that has attracted technological interest due to its tuned bandgap and lattice parameter features within a wide range [11]. The bandgap energy of $Zn_xCd_{1-x}S$ can be customized from 2.42eV (CdS) to 3.70eV (ZnS) depends on the amount of relative Zn content x. Also, $Zn_xCd_{1-x}S$ ensures a well-tuned conduction band alignment and provides tunable lattice parameters that can be closely matched with the absorbers by varying x [12]. Therefore, $Zn_xCd_{1-x}S$ based alternative buffer layer with a higher bandgap than CdS can be a promising approach in thin-film PV technology.

Typically a solar cell is grown layer by layer over a glass substrate, and the soda-lime glass is mostly used for thin-film PV technology, e.g., CIGS and CZTS based solar cells. CIGS or CZTS is a p-type absorber and CdS is a frequent n-type hetero partner, as described earlier. There are two extra layers (i:ZnO and Al:ZnO window layer) except the p-type absorber and n-type buffer layer. There are some rationales behind providing three n-type layers, including p-type absorber. The standard technique of fabricating ZnO and Al:ZnO is sputtering, which is a tough process involving the bombardment of high energy atoms at a considerable speed. Such a bombardment of high energy atoms may cause a detrimental effect on the absorber if ZnO is directly sputtered on the absorber. So a buffer layer of at least 10 nm must be fabricated by a soft process that doesn't relate to the bombardment of high energy atoms [13]. Also, the inclusion of the buffer layer prevents the Al diffusion from Al:ZnO layer into the absorber, which may change the characteristics of the absorber layer [14]. Therefore, buffer layer fabrication by chemical bath deposition is considered as a key milestone in the development of substrate type solar cells [15].

Numerous processes have been used to grow $Zn_xCd_{1-x}S$ thin-films containing spin coating [16], dip coating [17], electro-deposition [18, 19], chemical vapour deposition (CVD) [20], chemical bath deposition (CBD) [21-23], spray pyrolysis [24, 25], thermal evaporation [26], successive ionic layer adsorption and reaction (SILAR) [27], co-sputtering [28] and so on. Among the processes, CBD is mostly advantageous, e.g., inexpensive, simple non-vacuum, and low-temperature soft process, which has large scale deposition facilities and also is well suited for the manufacturing of solar cells in industrial scale. The properties of the $Zn_xCd_{1-x}S$ thin-films and nanostructures are strongly dependent on the fabrication method used and also to the processing steps, environments and post-deposition treatment [29]. Caijuan Tian et al. observed the improved structural properties of annealed (350°C at N_2 environment) $Zn_xCd_{1-x}S$ thin-films synthesized by CBD [22] and SD. Chavhan et al. demonstrated the effect of air annealing (400°C for 30 minutes) on the structural and optical properties of $Zn_xCd_{1-x}S$ (x=0 to 0.15) thin-films fabricated by CBD on ITO coated glass substrate [30]. A. Bakhsh et al. observed the improved structural and optical properties of vacuum annealed (300°C and 400°C) ZnCdS thin-films fabricated by close space sublimation process [31]. S. Kumar et al. also showed the improved both crystalline and optical properties of 400°C annealed ZnCdS thin-film fabricated by CBD [32]. In this essence, the effect of different annealing temperatures on the properties of $Zn_xCd_{1-x}S$ films has not been adequately discussed, regardless of the availability of various reports.

In this work, $Zn_xCd_{1-x}S$ (x=0 to 0.41) thin-films are synthesized by the CBD technique, and the structural and optical properties are analyzed. The as-deposited $Zn_{0.31}Cd_{0.69}S$ films are systematically annealed at different temperatures (200°C, 350°C and 500°C) in the N_2 environment. The annealed films are also analyzed to explore the possibility of applying it as an alternative buffer layer for solar cell applications.

2. Experimental

2.1. Materials and film growth

All experiments have been conducted in the cleanroom. Double deionized (DI) water was used for the experiments as well as for cleaning the glass substrates and instruments. Soda-lime glass (SLG) substrates were cleaned sequentially in methanol, acetone and DI water containing an ultrasound bath for 15 minutes. The substrates were then dried by the N_2 gas blower and finally on a hot plate. All the chemicals used in these experiments were as-received. Cadmium acetate dehydrate (Cd^{2+} source), zinc acetate dehydrate (Zn^{2+} source), Thiourea (S^{2-} source) and 28% wt. NH_4OH, as a complexing agent, was received from Merck Millipore, Germany, and was of ACS reagent grade. Chemical bath deposition of $Zn_xCd_{1-x}S$ thin-films was accomplished by using a cadmium source, a zinc source and a sulfur source solution. The composition of zinc in the fabricated sample was governed by changing the amount of zinc concentration in the bath solution. As a massive amount of zinc is being unreacted in the alkaline solution, so the amount of zinc content is needed to be much higher than the cadmium content in the bath solution. The reaction rate of both Cd^{2+} and Zn^{2+} is not the same in the alkaline solution and Cd^{2+} is much more reactive than Zn^{2+}. So the zinc concentration $[Zn^{2+}]$ in the chemical bath was gradually increased up to 4 times than the cadmium concentration $[Cd^{2+}]$, as stated in Table 1. The value of $x_{bath}=Zn/(Zn+Cd)|_{in\ bath}$ was varied from 0 to 0.83 to obtain different zinc content in the deposited samples. The CBD recipes used in these experiments were developed experimentally but, in some cases, based on some literature, publications and reasonable estimation [33-35].

The chemicals were poured into the reaction beaker according to the order, at the first complexing agent, then an aqueous solution (25 ml) of Cd^{2+} source and an aqueous solution (50 ml) of Zn^{2+} source one after the other and finally the aqueous solution (50 ml) of S^{2-} source. All the chemicals

were dissolved in DI water in separate conical flasks for at least 2 hours before starting the experiments.

Table 1. Deposition parameters for the fabrication of $Zn_xCd_{1-x}S$ thin-films by CBD

Exp. Code	Cadmium Acetate (gram)	Zinc Acetate (gram)	Thiourea (gram)	$[Zn^{2+}]/[Cd^{2+}]$ in bath
S01	0.40	0	1.50	0
S02	0.20	0.20	0.70	1
S03		0.40		2
S04		0.60		3
S05		0.80		4

The glass substrates were kept vertically inside the reaction beaker by using tweezers covered by Kapton tape. The experimental setup, as in Fig.1, contains 2 beakers, e.g., water bath beaker and reaction beaker. The reaction beaker contains chemical solutions kept into a hot water bath. The temperature of the water bath was maintained at ~65°C during experiments. All the experiments operated for 08 minutes after the nucleation had occurred. Also, a magnetic stirrer bar was rotated at a constant 600~700 rpm to mix all the reagents properly and also to remove bubbles from the surface of glass substrates. The temperature of both beakers was measured and recorded for every minute. After the deposition had finished, the coated glass substrates were transferred into a beaker containing 0.1M NH_4OH solution for a few seconds. After that, the coated films were transferred to running DI water to remove loosely bound particles. Shifting of the coated substrates into the solution of NH_4OH immediately after finishing the experiment is very important in the case of $Zn_xCd_{1-x}S$ deposition to avoid the formation of an unnecessary layer of $Zn(OH)_2$ [36]. Then the coated glass substrates were dried by blowing industrial nitrogen gas and stored into vacuum desiccator for further treatment and characterization.

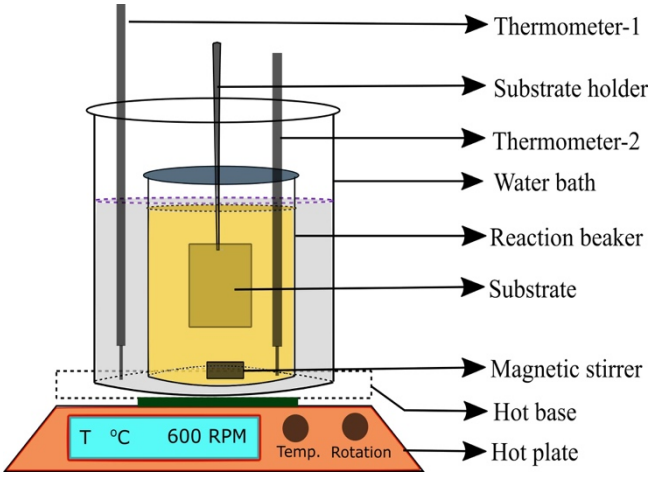

Fig. 1. Experimental setup for chemical bath deposition

The $Zn_{0.31}Cd_{0.69}S$ sample was chosen for further treatment and annealed at different temperatures (200°C, 350°C and 500°C) under N_2 ambient for 20 minutes with a ramp of 10°C per minute. The annealing process was performed at the tube furnace of a homemade closed space sublimation system. The tube pressure was maintained at 100 mTorr during the treatment. After the process had been completed, samples were cooled down naturally to room temperature and stored in the vacuum chamber.

2.2. *Film Characterization*

The Dektak stylus profilometer was used to measure the thickness of the as-grown films. The microstructural, optical, surface and elemental properties of the $Zn_xCd_{1-x}S$ films were investigated by X-ray diffractometer (XRD), Uv-Visible near-infrared (Uv-Vis N.I.R.) spectrophotometer, field emission scanning electron microscope (FESEM) and energy dispersive X-ray (EDX.) spectrometer respectively.

3. Results and discussions

3.1. *Film thickness*

Film thickness and T_{opc} (Time till opaque solution, T_{opc} is defined as the time when nucleation occurred and nothing else was seen through the solution of the beaker) as a function of comparative zinc content in the chemical bath, y is shown in Fig. 2.

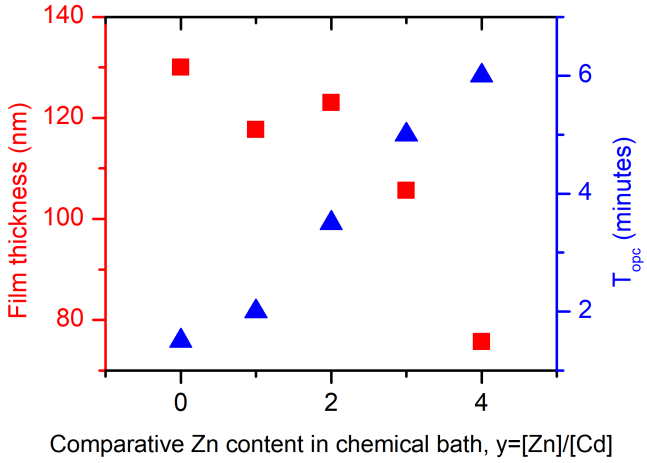

Fig. 2. Film thickness and T_{opc} as a function of Zn content chemical bath

Fig. 2 shows that T_{opc} is increased and film thickness is decreased for the incremental amount of zinc in the chemical bath. Although the deposition time after T_{opc} was fixed for all cases, the film thickness was reduced for the higher amount of zinc in the bath solution. The addition of zinc slows down the reaction rate and therefore, nucleation takes a little longer. So the film thickness had been observed a bit less for the films of higher zinc content.

3.2. *Elemental composition*

As many CBDs were performed to obtain different Zn content in the deposited $Zn_xCd_{1-x}S$ samples, so the elemental composition of the films was confirmed at first. The

elemental composition, as well as the atomic percentage of the deposited $Zn_xCd_{1-x}S$ (x=0, 0.25, 0.31, 0.36 and 0.41) thin-films from EDX. spectra are depicted in Fig. 3.

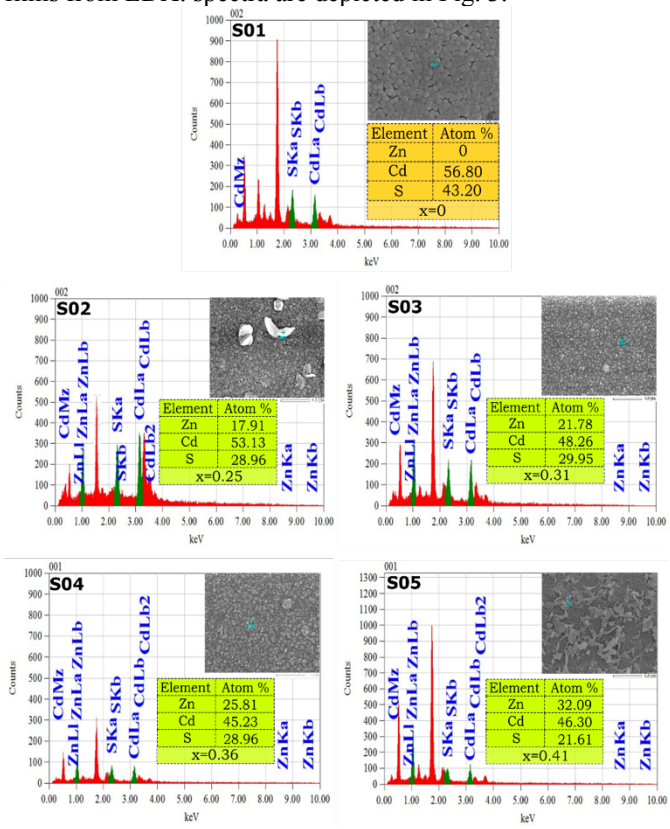

Fig. 3. EDX. spectra of as-grown $Zn_xCd_{1-x}S$ thin-films with the atomic percentage

Sharp peaks for Cd, Zn and S were found in the EDX. spectrum. Peaks at 0.50 keV and 1.75 KeV specified the existence of oxygen and silicon, respectively, which came from the glass substrate [30, 37]. The calculated relative zinc content, x is defined as the ratio of the atomic percentage of zinc to the total atomic percentage of zinc and cadmium in the deposited thin-films. Another term y is defined as the ratio of zinc concentration to cadmium concentration in the chemical bath solution. The relation between x and y is shown in Fig. 4.

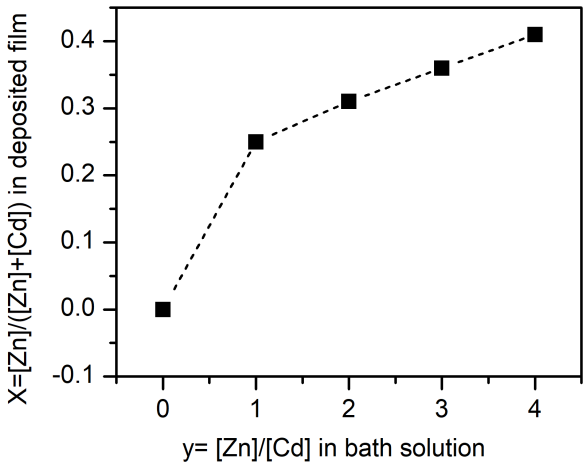

Fig. 4. Relation between relative zinc content in bath solution and deposited films

The plot of Fig.4 shows that the zinc content in the deposited $Zn_xCd_{1-x}S$ thin-films follows the incremental amount of zinc content in the bath solution. The relative zinc content x in the deposited sample is related proportionally to y. Variation of relative zinc content x=0 to 0.41 in the deposited sample was obtained by increasing the zinc content in the bath from 0 to 4 times than the cadmium content. But in reality, high zinc content in the bath solution doesn't mean the higher amount of zinc in the deposited films at the same rate due to the slow rate of formation of ZnS from Zn^{2+} than CdS from Cd^{2+} in the alkaline solution.

3.3. Microstructural and crystallographic properties

The microstructural properties of the as-grown $Zn_xCd_{1-x}S$ (x=0 to 0.41) thin-films were investigated by Philips/PANalytical X'Pert Pro-MPD Powder Diffractometer whose CuKα X-ray radiation wavelength is 0.154 nm. Fig. 5 shows the XRD patterns of the as-grown $Zn_xCd_{1-x}S$ thin-films on soda-lime glass substrates. The standard XRD data of the CdS (002) plane with diffraction peak at 2θ=26.507° and ZnS (002) plane with diffraction peak at 2θ=28.50° is used as a reference.

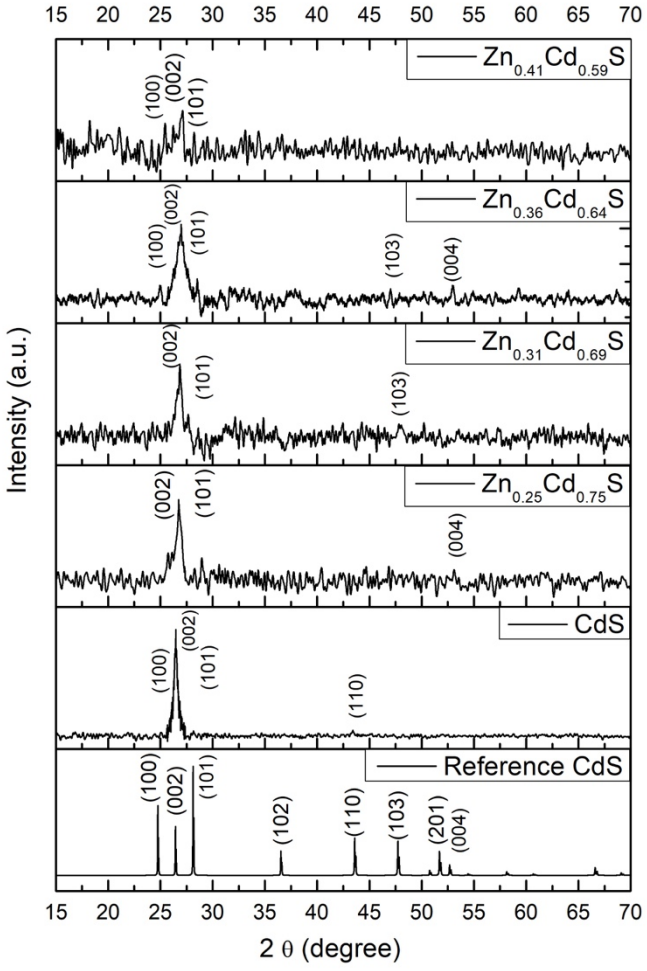

Fig. 5. XRD spectra of as-deposited $Zn_xCd_{1-x}S$ (x=0 to 0.41) thin-films

The chemical bath deposited $Zn_xCd_{1-x}S$ films are naturally

Table 2. Summary of structural properties of as-grown $Zn_xCd_{1-x}S$ thin-films

$Zn_xCd_{1-x}S$ Sample	Bragg angle, 2θ (degree)	Avg. Crystallite Size (nm)	Micro Strain, ε ($*10^{-3}$)	Lattice Constant, (Å)		Dislocation Density, δ ($\times 10^{11}$ cm^{-2})
				a	C	
0	26.49	25.66	5.89	4.12	6.73	0.84
0.25	26.75	14.35	10.59	4.08	6.66	2.75
0.31	26.85	13.01	11.47	4.06	6.63	3.26
0.36	27.01	11.26	13.19	4.04	6.60	4.35
0.41	27.12	9.66	15.30	4.02	6.56	5.90

very thin (~100nm) and don't show any remarkable peaks from any planes except (002). The same phenomena were observed at NREL technical report [33]. The XRD spectra of the as-deposited films have diffraction peaks for (002), (101), (100), (103) and (004) planes suggest that the as-deposited $Zn_xCd_{1-x}S$ has wurtzite structure (hexagonal). The sharp peak at near 2θ=26.49° corresponding to (002) plane, and other peaks are inconsiderable as compared to the main peak. The peaks become weaker when zinc is added in the bath solution because of the amorphous nature of the zinc-rich material. Also, the 2θ angle is shifted to the right for incremental values of x as compared to CdS. The crystallographic parameters are depicted in Table 2 using Bragg's law, crystal geometry and Debye-Scherrer formula [38-42] as in equation (1) - (6).

$$2d_{hkl}\sin\theta = n\lambda \tag{1}$$

$$\frac{1}{d_{hkl}^2} = \frac{4}{3}\left(\frac{h^2+hk+k^2}{a^2}\right)+\frac{l^2}{c^2} \tag{2}$$

$$C_{hex} = a_{hex}\times\sqrt{\frac{8}{3}} \tag{3}$$

$$\text{Crystallite size, } D_{hkl} = \frac{0.9\lambda}{\beta_{hkl}\times\cos\theta} \tag{4}$$

$$\text{Micro-strain, } \varepsilon = \frac{\beta_{hkl}}{4\tan\theta} \tag{5}$$

$$\text{Dislocation density, } \delta = \frac{15\varepsilon}{\alpha D_{hkl}} \tag{6}$$

Here d_{hkl} and D_{hkl} are the interatomic distance and crystallite size of a particular crystal plane (hkl), *a* and C are lattice constant, λ is the wavelength of incident X-ray (CuK_α radiation, 0.15406 nm), β_{hkl} is full-width half maxima for a given diffraction peak, and 2θ is the diffraction angle. The crystal plane is (002) ≡ (hkl) for ~26.50°, which is confirmed from JCPDS standard data card. Putting (hkl) values into the equation of the hcp system, the calculated value of C for (002) plane is 2d.

The data of lattice parameters for different relative zinc content as in Table 2 show that the calculated lattice parameters from experimental data are very close to the ideal material properties. In response to the Vegard's law, the value of lattice parameters of $Zn_xCd_{1-x}S$ (x=0 to 0.41) films is in between the lattice parameter of CdS and ZnS according to a linear combination based on the value of x [43, 44].

Stress and strain in functional thin-films can be correlated to the presence of extended structural defects such as dislocations and grain boundaries, which affect the performance of a semiconductor device composed of a stack thin-film layers one after another. Crystallite size is being smaller for $Zn_xCd_{1-x}S$ samples as zinc content increases. Also, the micro-strain and dislocation density are quite higher for $Zn_xCd_{1-x}S$ samples than CdS because thinner films have more significant grain boundaries per unit area that lead to an increase in micro-strain. The formation of larger crystallite by increasing thickness leads to a small area of grain boundaries per unit area.

3.4. Optical properties

Optical transmittance and absorbance spectra of as-deposited $Zn_xCd_{1-x}S$ (x=0 to x=0.41) thin-films were measured at room temperature using HITACHI U-2900 UV-Vis NIR spectrophotometer. Optical transmittance firmly relates to the structure of the deposited films as well as fabrication technique, process parameters, and also to the thickness of the films. Fig. 6 shows the transmittance spectra of the as-grown $Zn_xCd_{1-x}S$ thin-films of relative zinc content x=0 to 0.41 over the wavelength region of 300nm to 1100nm.

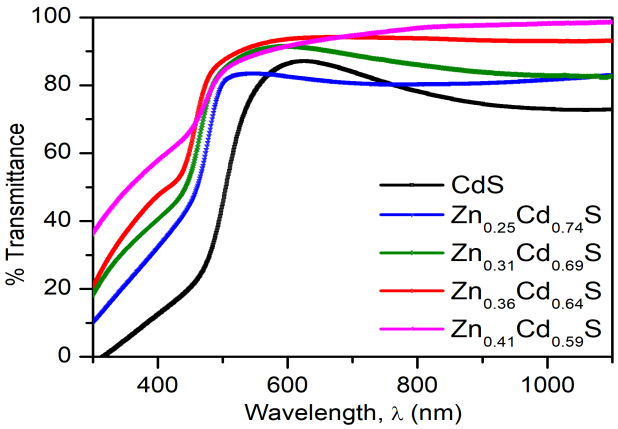

Fig. 6. Optical transmittance spectra of $Zn_xCd_{1-x}S$ (x=0 to 0.41) thin-films

All the $Zn_xCd_{1-x}S$ (x=0.26, 0.31, 0.36 and 0.41) thin-films

show superior transmittance over the entire region of wavelength as compared to the transmittance of as-deposited CdS thin-film. The average transmittance of $Zn_xCd_{1-x}S$ thin-films is ~80- 90% over the wavelength region of 500nm to longer wavelengths, which is relevant for applying $Zn_xCd_{1-x}S$ thin-films as a good buffer layer for solar cell applications. Besides, a remarkable amount of increment in transmittance over the blue region of sun spectrum (~ 400-500 nm) is observed for the as-deposited $Zn_xCd_{1-x}S$ thin-films. This desirable feature enhances the short circuit current density (J_{sc}) as well as improves the quantum efficiency in the blue wavelength region by reducing the amount of photon absorption in the buffer layer and passing more photons towards the absorber layer which effectively contribute to the generation of photogenerated carriers.

The absorption coefficient, α of the films can be calculated from the absorbance spectra. The following relation as in equation (7) is used to estimate the values of α(λ) in the strong absorption region of the absorbance spectra.

$$\alpha(\lambda) = \frac{1}{d} A(\lambda) = \frac{1}{d}(2 - \log_{10}\%T(\lambda)) \quad (7)$$

Where d means film thickness and A is the absorbance of the deposited films on a single side of the substrate. Absorbance A can also be calculated from the transmittance spectra, according to Beer-Lambert law.

Wavelength dependent absorption coefficient, α (λ) in m^{-1}, is directly related to the extinction coefficient, K, which refers to the decaying factor when light travels through a material according to equation (8).

$$\frac{P(x=d)}{P(x=0)} \propto \frac{E^2(x=d)}{E^2(x=0)} = e^{\frac{-4\pi fkd}{C}} = e^{-\alpha d} \quad (8)$$

Where P(x=0) and P(x=d) means the power of incident light at the moment of entering into the material and power after traveling a distance of d respectively. The term E denotes the light intensity, f is the incident light frequency, c is the velocity of light and k is the extinction coefficient. Wavelength dependent absorption coefficient, α (λ) of the as-grown $Zn_xCd_{1-x}S$ thin-films is shown in Fig. 7

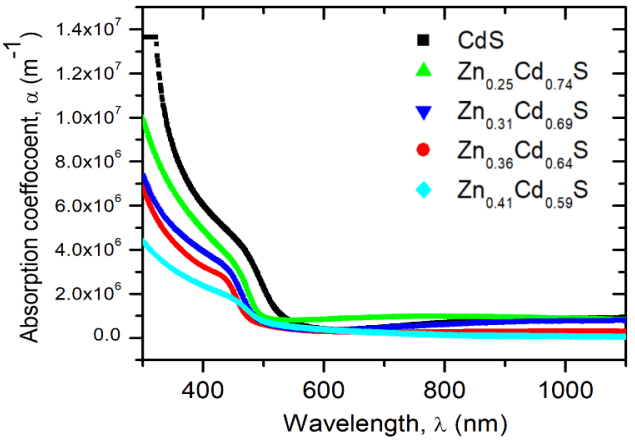

Fig. 7. Absorption coefficient spectra of as-grown $Zn_xCd_{1-x}S$ (x=0 to 0.41) thin-films

Fig.7 shows that the absorption coefficient tends to decrease for the zinc-rich films. Films having a low absorption coefficient are recommended as a good buffer layer because light intensity inside the solar cell is related to the absorption coefficient according to the inverse exponential function, as in equation (8).

The low absorption coefficient offers less decay of light in the buffer layer and allows more photons to enter towards the absorber layer, which is a crucial parameter to improve the short circuit current density (J_{sc}) as well as photoconversion efficiency. Optical bandgap energy (E_g) of the deposited films can be estimated according to the relation described by J. Touc as in equation (9) [45].

$$\alpha h\nu \propto (h\nu - E_g)^n \quad (9)$$

Where the value of n is 2 or 3, α is the absorption coefficient, h is Planks constant and ν is photon frequency. Fig. 8 shows the plot of $(\alpha h\nu)^2$ versus the photon energy, hν of $Zn_xCd_{1-x}S$ thin-films.

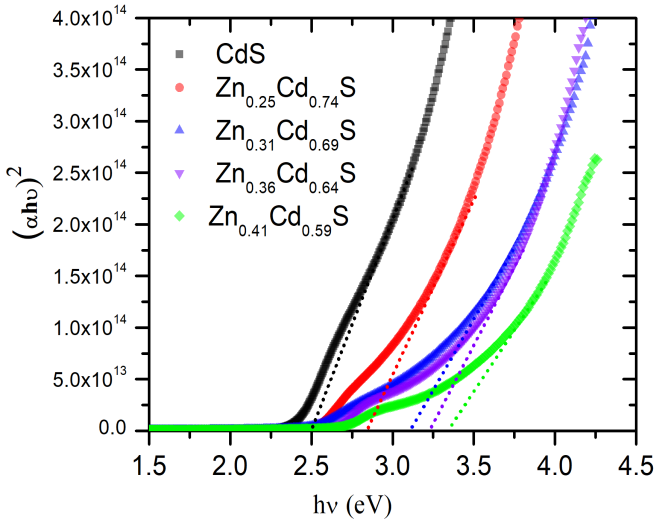

Fig. 8. Tauc plot of as-deposited $Zn_xCd_{1-x}S$ (x=0 to 0.41) thin-films

It is clear from Fig. 8 that the absorption edges shift to the higher photon energy region as the relative zinc content increases. The result reveals that the optical band gap energy is increased with higher relative zinc content in the $Zn_xCd_{1-x}S$. By extrapolating the straight-line portion of the plot of Fig.8 in the high α region (α >10^6 m^{-1}), the optical band gap values are extracted and reported in Fig. 9 as a function of relative zinc content x.

The optical bandgap of the as-deposited $Zn_xCd_{1-x}S$ films increases from 2.50 eV to 3.35 eV as the values of zinc content increases in the films from x=0 to x=0.41. The overall effect is that the incorporation of zinc in CdS leads to a remarkable improvement in optical transmittance in the blue region as well as in the higher wavelength region and also increases the optical bandgap of the $Zn_xCd_{1-x}S$ films up to 3.35eV for relative zinc content x=0.41.

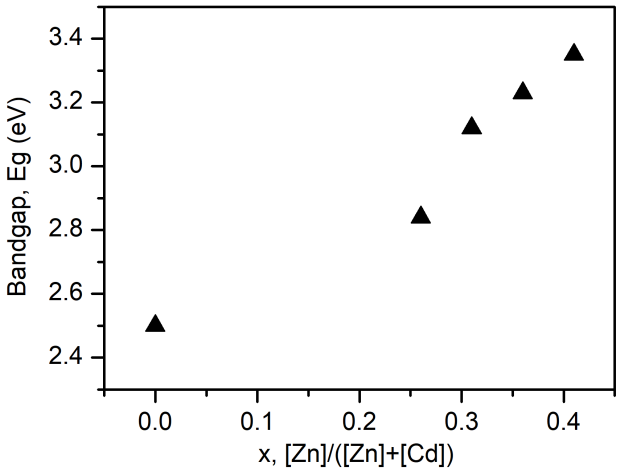

Fig. 9. Composition dependent bandgap of as-deposited $Zn_xCd_{1-x}S$ thin-films

3.5. *Surface morphology*

In Fig. 10, shows the plan view FESEM images of the deposited $Zn_xCd_{1-x}S$ samples for different values of x.

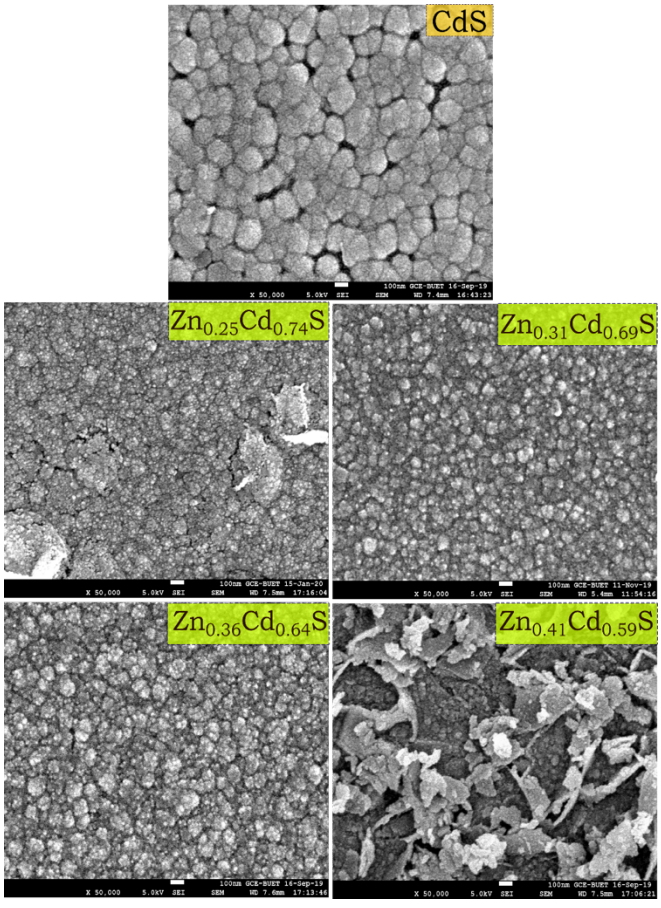

Fig. 10. Surface micrographs of as-deposited $Zn_xCd_{1-x}S$ (x=0 to 0.41) thin-films

The FESEM micrographs provide important information about the growth mechanism, size, and shape of the grains. It is inspected that all the $Zn_xCd_{1-x}S$ films have no pinholes and voids. The average grain size of the as-grown films is calculated by using ImageJ software according to the mean linear intercept method. The grain size of $Zn_xCd_{1-x}S$ films is increased with higher relative zinc content up to x=0.36, and beyond the value, grain size is tended to decrease. The calculated grain size are approximately in the range of 98 nm- 114 nm (average ~107 nm ± 8 nm) for CdS, 50 nm-55nm (average ~52 nm ±3 nm) for $Zn_{0.25}Cd_{0.75}S$, 51 nm- 61 nm (average ~ 56 nm ± 5 nm) for $Zn_{0.31}Cd_{0.69}S$, 63 nm-76 nm (average ~ 70 nm ± 6 nm) for $Zn_{0.36}Cd_{0.64}S$ and 27 nm – 32 nm (average ~ 31 nm ± 3nm) for $Zn_{0.41}Cd_{0.59}S$. The surface of $Zn_xCd_{1-x}S$ samples is comparatively smooth, and nano-crystalline grains (<100nm) are formed. Variation in grain size may be caused by the difference in nucleation process and reaction rate as different zinc content in the bath solution changes the reaction rate and nucleation time.

3.6. *Effect of thermal annealing*

Characterization and analysis of the as-grown films reveal that the $Zn_xCd_{1-x}S$ (x=0.31 and 0.36) samples show relatively good structural and optical properties among the $Zn_xCd_{1-x}S$ samples along with the smooth and compact surface properties without any pinholes or voids. Also, $Zn_xCd_{1-x}S$ thin-films with relative zinc content x=0.30 to 0.40 have been termed as the best suited alternative buffer layer for conventional CZTS/CdS and CIGS/CdS solar cells [27, 33]. So, $Zn_{0.31}Cd_{0.69}S$ was chosen for further treatment and annealed at different temperatures (200°C, 350°C and 500°C) under N_2 ambient of 100 mTorr for 20 minutes. The colour variation of the as-deposited and annealed films are shown in Fig. 11. The as-grown and annealed $Zn_{0.31}Cd_{0.69}S$ films show smooth and homogeneous coating over the substrate area. It is observed that the $Zn_{0.31}Cd_{0.69}S$ film is lighter in colour as compared to the CdS film, which indicates the high transparency of $Zn_{0.31}Cd_{0.69}S$ than CdS. Also, the colour of the annealed $Zn_{0.31}Cd_{0.69}S$ films is getting a little darker at 200°C annealing temperature, and then it is back to light colour at 350°C and 500°C annealing temperatures.

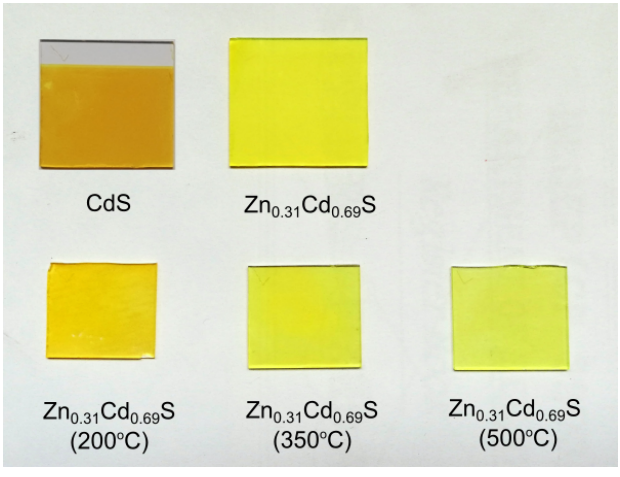

Fig. 11. The colour variation of as-grown and annealed $Zn_xCd_{1-x}S$ thin-films

The X-ray diffraction spectra of the annealed $Zn_{0.31}Cd_{0.69}S$ thin-films at different temperatures are shown in Fig. 12. The Bragg angle, 2θ position initially shifts to the left for 200°C annealing temperature and gradually shift to the right for

higher annealing temperature at 350°C and 500°C. 100% relative peak intensity for (002) plane is obtained at 350°C temperature indicates a strong orientation of crystals along (002) plane. Peak intensities increase up to 350°C and then decrease at higher temperatures.

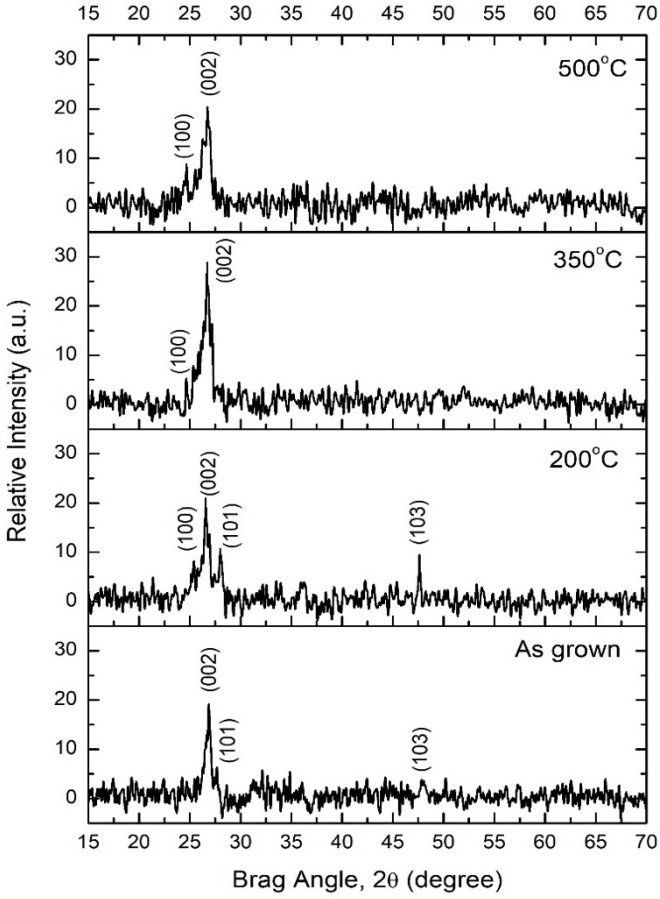

Fig. 12. XRD spectra of as-grown and annealed $Zn_{0.31}Cd_{0.69}S$ thin-films

At 200°C annealing temperature, mixed phases of (100)h, (002)h, (101)h and (103)h are found which indicates the random orientation of crystals in the film. Meanwhile, increasing the annealing temperature at 350°C, the orientation of crystals along (002) plane becomes stronger than the 200°C annealed film and also the orientation along (101) and (103) plane disappears. As we further increase the annealing temperature at 500°C, then the peak is widened and the intensity is decreased along (002) plane which probably due to the more diffusion of zinc at higher annealing temperature [31]. The calculated crystallographic properties and lattice constants of the annealed $Zn_{0.31}Cd_{0.69}S$ films at different temperatures are shown in Table 3.

The crystallographic data of Table 3 reveals that the crystallite size increases, and as well as an improvement in micro-strain and dislocation density are observed for the films annealed up to 350°C temperature and thereafter the properties are declined at a higher annealing temperature of 500°C. The 350°C annealed film shows a better crystallinity along with a sharp dominant peak from (002) plane in comparison to the other films due to the proper orientation along (002) plane. Also, considering the disappearance of (101) and (102) planes at 350°C causes a reduction in micro-strain, dislocations and lattice misfits from these two planes. Hence the 350°C annealed film shows lower micro-strains and dislocation density as compared to the others.

The lattice constant values are increased due to annealing as compared to the as-grown $Zn_{0.31}Cd_{0.69}S$ thin-film. The highest value of 4.11Å is calculated for 200°C annealed films and after that, the value is decreased but still quite higher than the as-grown sample. The increment of lattice constant in the annealed films at elevated temperature indicates the formation of compressive strain in the direction of the film growth plane [46, 47].

Optical transmittance spectra of the as-grown and annealed $Zn_{0.31}Cd_{0.69}S$ thin-films at different temperatures are shown in Fig. 13.

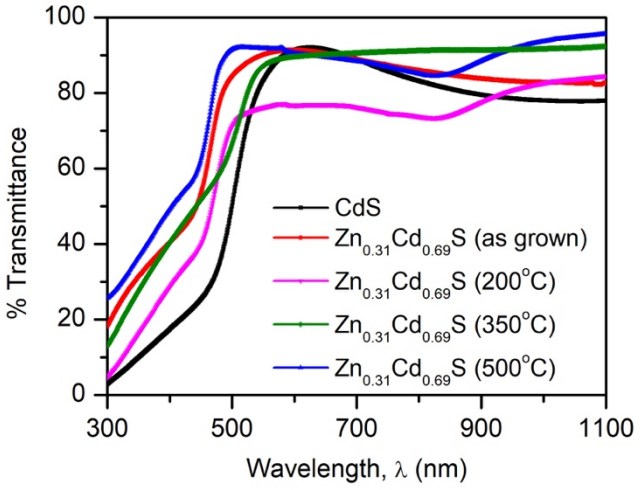

Fig. 13. Optical transmittance spectra of the annealed $Zn_{0.31}Cd_{0.69}S$ thin-films

Fig. 13. Shows that the transmittance is primarily reduced at 200°C annealing temperature over the whole spectrum and

Table 3. Summary of microstructural properties of annealed $Zn_{0.31}Cd_{0.69}S$ thin-films

Sample	Bragg angle 2θ (deg.)	Relative peak intensity (%)	Avg. crystalline size (nm)	Micro strain, ε (*10^{-3})	Lattice constant, (Å)		Dislocation density,δ (×10^{11} cm^{-2})
					a	C	
$Zn_{0.31}Cd_{0.69}S$(as-grown)	26.85	66.28	12.81	11.66	4.06	6.63	3.36
$Zn_{0.31}Cd_{0.69}S$(200°C)	26.57	72.8	14.32	10.53	4.11	6.71	2.69
$Zn_{0.31}Cd_{0.69}S$(350 °C)	26.69	100	17.37	8.64	4.09	6.68	1.83
$Zn_{0.31}Cd_{0.69}S$(500 °C)	26.72	70.83	9.96	15.07	4.08	6.66	5.56

after that, the improvement in the transmittance (average ~ 90%) is observed for the annealed films at both 350°C and 500°C. The reduction in transmittance at 200°C may cause due to the recrystallization of the films, increment in crystallite size and elimination of some numerous voids. Also, the absorption edges are lied in between 400nm to 500nm for all the annealed films.

The optical energy band gap of the annealed $Zn_{0.31}Cd_{0.69}S$ thin-films at different temperatures is calculated, and the corresponding Tauc plots are assembled in Fig. 14. The bandgap is initially observed to decrease for the annealed films at 200°C and then gradually increase at 350°C and 500°C.

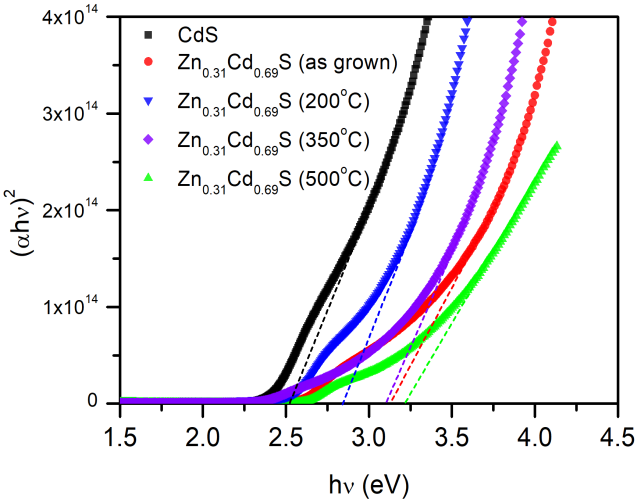

Fig. 14. $(\alpha h\nu)^2$ versus hν polts of the annealed $Zn_{0.31}Cd_{0.69}S$ thin-films

There are several reasons behind the variation of bandgap at different annealing temperatures. The bandgap of the annealed film at 200°C may have been decreased due to the improvement in crystallinity and lattice structure as compared to the as-grown film [48, 49].

In structural studies, we observed the right shift of dominant (002) plane at higher annealing temperatures of 350°C and 500°C that indicates the phase transition from hexagonal to cubic and hence the improvement in optical bandgap at 350°C was observed due to the phase transition along with the improvement in crystallinity [49, 50]. Further improvement in optical bandgap at 500°C may be caused due to the diffusion of zinc [31] and as well as the crystallinity was decreased which is consistent with the XRD spectral analysis of as-grown $Zn_xCd_{1-x}S$ thin-films.

Also, dominating the CdS phase along with the better crystal orientation in multiple planes may be the possible reason behind the colour darkening of the $Zn_{0.31}Cd_{0.69}S$ film at 200°C annealing temperature. At 200°C annealing temperature, the dominant (002) XRD peak shifts to the left (26.57° which is nearer to the (002) XRD peak of CdS) as compared to the as-grown sample from which the dominance of the CdS phase can be determined. Hence the 200°C annealed film is little darker as well as the colour is very close to the CdS film which is consistent with the reduction in transmittance and bandgap as observed in Fig. 13 and Fig. 14.

The optical energy band gap of as-deposited $Zn_{0.31}Cd_{0.69}S$ thin-film is 3.12eV. The estimated optical band gap values of annealed $Zn_{0.31}Cd_{0.69}S$ thin-films are 2.85eV, 3.10eV and 3.22eV for annealing temperatures 200°C, 350°C and 500°C respectively as in Fig. 15.

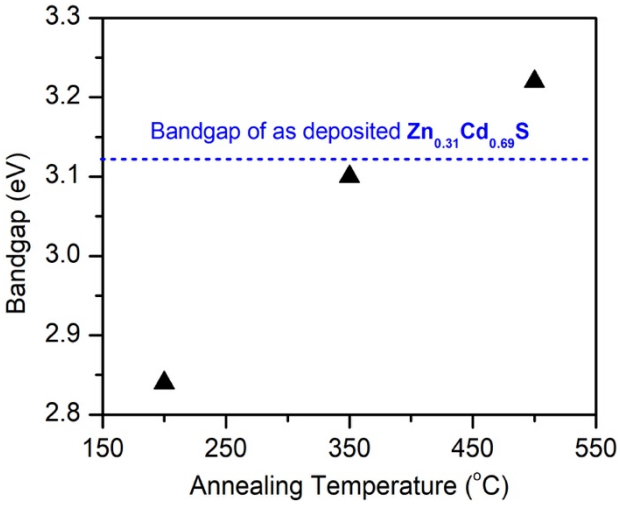

Fig. 15. Bandgap of $Zn_{0.31}Cd_{0.69}S$ thin-films at different annealing temperature

Incorporation of zinc in CdS thin-film degrades the crystalline properties of the films indeed and on the other hand, optical properties, as well as bandgap are enhanced with an incremental amount of zinc. Post deposition annealing treatment improves the crystallinity of the annealed $Zn_{0.31}Cd_{0.69}S$ film. Annealed $Zn_{0.31}Cd_{0.69}S$ thin-film at 350°C temperature offers the best crystallinity (more improved than as-grown $Zn_{0.31}Cd_{0.69}S$ film) without compromising the optical properties. So from the systematic annealing treatment (200°C, 350°C and 500°C), $Z_{0.31}Cd_{0.69}S$ thin-film annealed at 350°C with improved crystalline and optical properties (improved blue and long-wavelength response) can be treated as a good alternative of conventional CdS buffer layer in thin-film solar cell applications.

4. Conclusion

In summary, we have synthesized $Zn_xCd_{1-x}S$ (x=0 to 0.41) thin-films by CBD, and the structural and optical properties have been analyzed. It has been observed that due to the amorphous nature of ZnS and therefore the partial replacement of cadmium with different amounts of zinc gradually reduced the crystallinity of the $Zn_xCd_{1-x}S$ thin-films. On the other hand, with the increase in zinc content, there has been a significant improvement in optical properties with a substantial blue shift having an energy bandgap of 2.50eV to 3.35eV for x=0 to 0.41. Therefore, the $Zn_{0.31}Cd_{0.69}S$ sample has been annealed at 200°C, 350°C and 500°C temperature for the improvement of crystallinity. Besides, the structural and optical properties of the annealed films are investigated. In the case of annealed $Zn_{0.31}Cd_{0.69}S$ films, the transmittance and as well as the bandgap are initially reduced at 200°C temperature as compared to the as-grown sample but at a higher annealing temperature of 350°C

and 500°C, both the transmittance and bandgap started to increase again. The bandgap of 3.10eV has been obtained for the 350°C annealed $Zn_{0.31}Cd_{0.69}S$ film, whereas the bandgap of the as-grown film is 3.12eV. Also, the best crystallinity has been achieved for the 350°C annealed $Zn_{0.31}Cd_{0.69}S$ film. So it can be said that annealing of $Zn_{0.31}Cd_{0.69}S$ thin-film at temperatures around 350°C makes it possible to achieve good crystallinity without any loss of optical transmittance and bandgap values. Considering the analysis of structural and optical properties, $Zn_{0.31}Cd_{0.69}S$ thin-film annealed at temperatures around 350°C can be suggested as a good alternative buffer layer for CIGS, CZTS and CdTe based thin-film solar cells.

Acknowledgement

We would like to express our gratitude to Department of Electrical and Electronic Engineering (EEE) and Directorate of Research and Extension (DRE) of Chittagong University of Engineering and Technology (CUET), Chattogram-4349, Bangladesh for providing research funds through HEQEP (CP-3200) and CUET/DRE/2018-19/EEE-006 projects and Materials Science Division, Atomic Energy Centre, Dhaka for providing the characterization support.

References

[1] H. Sun, S. Lin, R. Zhang, K. Yang, M. Xia, W. Li, W. Guo, "Perovskite solar cells employing Al_2O_3 scaffold layers", 2014 International Conference on Renewable Energy Research and Application (ICRERA), Milwaukee, WI, pp. 442-444, 2014. (Conference paper)

[2] N. K. Kasim, H. H. Hussain, A. N. Abed, "Performance Analysis of Grid-Connected CIGS PV Solar System and Comparison with PVsyst Simulation Program", International Journal of Smart Grid, Vol.3, No.4, pp. 172- 179, December, 2019. (Article)

[3] A. C. Busacca, V. Rocca, L. Curcio, A. Parisi, A. C. Cino, R. Pernice, A. Andò, G. Adamo, A. Tomasino, G. Palmisano, S. Stivala, M. Caruso, G. Cipriani, D. La Cascia, V. Di Dio, G. Ricco Galluzzo and R. Miceli "Parametrical study of multilayer structures for CIGS solar cells", 2014 International Conference on Renewable Energy Research and Application (ICRERA), Milwaukee, WI, pp. 964-968, 2014. (Conference paper)

[4] S. Chavhan, R. P. Sharma, "Growth, structural and optical transport properties of nanocrystal $Zn_{1-x}Cd_xS$ thin films deposited by solution growth technique (SGT) for photosensor applications", J. Phys. Chem. Solids, vol. 66, no. 10, pp. 1721–1726, 2005. (Article)

[5] M.S. Hossain, M.A. Islam, M.M. Aliyu, P. Chelvanathan, T. Razykov, K. Sopian, N. Amin, "Effect of annealing on the properties of $Zn_xCd_{1-x}S$ thin film growth by RF magnetron co-sputtering", Energy Procedia, vol. 33, pp. 214–222, 2013. (Article)

[6] N.K. Das, J. Chakrabartty, S.F.U. Farhad, A.K. Sen Gupta, E.M.K. Ikball Ahamed, K.S. Rahman, A. Wafi, A.A. Alkahtani, M.A. Matin, N. Amin, "Effect of substrate temperature on the properties of RF sputtered CdS thin films for solar cell applications", Results in Physics, vol. 17, pp. 0–7, June 2020. (Article)

[7] M.M. Islam, S. Ishizuka, A. Yamada, K. Sakurai, S. Niki, T. Sakurai, K. Akimoto, "CIGS solar cell with MBE-grown ZnS buffer layer", Sol. Energy Mater. Sol. Cells, vol. 93, no. 6–7, pp. 970–972, 2009. (Article)

[8] T. Nakada and M. Mizutani, "18% efficiency Cd-free $Cu(In,Ga)Se_2$ thin-film solar cells fabricated using chemical bath deposition (CBD)-ZnS buffer layers", Japanese J. Appl. Physics, Part 2 Lett., vol. 41, no. 2 B, pp. 7–10, 2002. (Article)

[9] M. Nakamura, K. Yamaguchi, Y. Kimoto, Y. Yasaki, T. Kato and H. Sugimoto, "Cd-Free $Cu(In,Ga)(Se,S)_2$ thin-film solar cell with record efficiency of 23.35%", IEEE J. Photovoltaics, vol. 9, no. 6, pp. 1863–1867, 2019. (Article)

[10] D. Bae, J. Gho, M. Shin and S. Kwon, "Effect of zinc addition on properties of cadmium sulfide layer and performance of $Cu(In,Ga)Se_2$ solar cell", Thin Solid Films, vol. 535, no. 1, pp. 162–165, 2013. (Article)

[11] W. E. Devaney, W. S. Chen, J. M. Stewart and R. A. Mickelsen, "Structure and Properties of High Efficiency $ZnO/CdZnS/CuInGaSe_2$ Solar Cells", IEEE Trans. Electron Devices, vol. 37, no. 2, pp. 428–433, 1990. (Article)

[12] A. Baran, "Chemical bath deposited zinc cadmium sulfide and sputter deposted zinc oxide for thin film solar cell device fabrication", University of Florida , 2009. (Reports)

[13] D. Hironiwa, N. Matsuo, N. Sakai, T. Katou, H. Sugimoto, J. Chantana, Z. Tang and T. Minemoto, "Sputtered (Zn,Mg)O buffer layer for band offset control in $Cu_2ZnSn(S,Se)_4$ solar cells", Jpn. J. Appl. Phys., vol.53, no.10, pp. 106502-1-6, 2014. (Article)

[14] L. C. Olsen, P. Eschbach, S. Kundu and D. J. Gaspar, "Role of buffer layers in CIS-based solar cells", Conf. Rec. IEEE Photovolt. Spec. Conf., pp. 652–655, 2002. (Conference paper)

[15] R. Scheer, H. W. Schock, Chalcogenide Photovoltaics, Wiley-VCH Verlag GmbH & Co. KGaA, 2011, pp. 235-273.(Book)

[16] A. A. K. Bakly, B. F. Spencer and P. O'Brien, "The deposition of thin films of cadmium zinc sulfide $Cd_{1-x}Zn_xS$ at 250 °C from spin-coated xanthato complexes: a potential route to window layers for photovoltaic cells", J. Mater. Sci., vol. 53, no. 6, pp. 4360–4370, 2018. (Article)

[17] M. K. Karanjai and D. Dasgupta, "Preparation and study of sulphide thin films deposited by the dip technique", Thin Solid Films, vol. 155, no. 2, pp. 309–315, 1987. (Article)

[18] M. N. Mammadov, A. Sh Aliyev and M. Elrouby, "Electrodeposition of Cadmium Sulfide", Int. J. Thin

Film Sci. Tec, vol. 1, no. 2, pp. 43–53, 2012. (Article)

[19] S. Azmi, M. Nohair, M. El Marrakchi, E. M. Khoumri and M. Dabala, "Effect of the Complexing Agents on the Properties of Electrodeposited CZTS Thin Films", 2018 7th International Conference on Renewable Energy Research and Applications (ICRERA), Paris, pp. 1346-1351, 2018. (Conference Paper)

[20] D. Barreca, A. Gasparotto, C. Maragno, R. Seraglia, E. Tondello, A. Venzo, V. Krishnan and H. Bertagnolli, "Cadmium O-alkylxanthates as CVD precursors of CdS: a chemical characterization", Appl. Organomet. Chem., vol. 19, no. 1, pp. 59–67, 2005. (Article)

[21] J. N. Alexander, S. Higashiya, D. Caskey, H. Efstathiadis and P. Haldar, "Deposition and characterization of cadmium sulfide (CdS) by chemical bath deposition using an alternative chemistry cadmium precursor", Sol. Energy Mater. Sol. Cells, vol. 125, pp. 47–53, 2014. (Article)

[22] C. Tian, J. Gao, W. Li, L. Feng, J. Zhang and L. Wu, "$Cd_{1-x}Zn_xS$ thin films with low zn content prepared by chemical bath deposition", Int. J. Photoenergy, vol. 2012, pp. 3–8, 2012. (Article)

[23] B. S. Tosun, C. Pettit, S. A. Campbell and E. S. Aydil, "Structure and composition of $Zn_xCd_{1-x}S$ films synthesized through chemical bath deposition", ACS Appl. Mater. Interfaces, vol. 4, no. 7, pp. 3676–3684, 2012. (Article)

[24] M. C. Baykul and N. Orhan, "Band alignment of $Cd_{(1-x)}Zn_xS$ produced by spray pyrolysis method", Thin Solid Films, vol. 518, no. 8, pp. 1925–1928, 2010. (Article)

[25] N. D. Sankır, E. Aydın and E. Uğur, "Spray pyrolized copper indium gallium sulfide abosrober layers for thin film solar cells", 2013 International Conference on Renewable Energy Research and Applications (ICRERA), Madrid, pp. 559-561, 2013. (Conference Paper)

[26] J. H. Lee, W. C. Song, J. S. Yi, K. J. Yang, W. D. Han and J. Hwang, "Growth and properties of the $Cd_{1-x}Zn_xS$ thin films for solar cell applications", Thin Solid Films, vol. 431–432, no. 03, pp. 349–353, 2003. (Article)

[27] K. Sun, C. Yan, F. Liu, J. Huang, F. Zhou, J. A. Stride, M. Green and X. Hao, "Over 9% Efficient Kesterite Cu_2ZnSnS_4 Solar Cell Fabricated by Using $Zn_{1-x}Cd_xS$ Buffer Layer", Adv. Energy Mater., vol. 6, no. 12, pp. 4–9, 2016. (Article)

[28] M.S. Hossain, K.S. Rahman, M.A. Islam, M. Akhtaruzzaman, H. Misran, M.A. Alghoul, N. Amin, "Growth optimization of $Zn_xCd_{1-x}S$ films on ITO and FTO coated glass for alternative buffer application in CdTe thin film solar cells", Optical Mateials, vol. 86, pp. 270–277, 2018. (Article)

[29] K. Ramasamy, M. A. Malik, N. Revaprasadu and P. O'Brien, "Routes to nanostructured inorganic materials with potential for solar energy applications", Chem. Mater., vol. 25, no. 18, pp. 3551–3569, 2013. (Article)

[30] S. D. Chavhan, S. Senthilarasu and S. H. Lee, "Annealing effect on the structural and optical properties of a $Cd_{1-x}Zn_xS$ thin film for photovoltaic applications", Appl. Surf. Sci., vol. 254, no. 15, pp. 4539–4545, 2008. (Article)

[31] Y. C. A. Bakhsh, I. H. Gul, A. Maqsood, C. H. Chan, S. H. Wu, Yia Chang, "Tailoring the structural and optical properties of CdZns thin films by vacuum annealing", Chalcogenide Lett., vol. 13, no. October, pp. 443–450, 2016. (Article)

[32] S. Kumar, S. Rajpal, S. K. Sharma, D. Roy and S. R. Kumar, "Effect of Zn concentration on the structural, morphological and optical properties of ternary ZnCdS nanocrystalline thin films", Dig. J. Nanomater. Biostructures, vol. 12, no. 2, pp. 339–347, 2017. (Article)

[33] V. Craciun, Fundamental Materials Research and Advanced Process Development for Thin-Film CIS-Based Photovoltaics, Final Technical Report, NREL, 2006. (Reports)

[34] M. A. Contreras, M. J. Romero, B. To, F. Hasoon, R. Noufi, S. Ward, K. Ramanathan, "Optimization of CBD CdS process in high-efficiency $Cu(In,Ga)Se_2$-based solar cells", Thin Solid Films, vol. 403–404, pp. 204–211, 2002. (Article)

[35] K. M. McPeak, B. Opasanont, T. Shibata, D. Kyun Ko, M. A. Becker, S. Chattopadhyay, H. P. Bui, T. P. Beebe, Jr., B. A. Bunker, C. B. Murray and J. B. Baxter, "Microreactor Chemical Bath Deposition of Laterally Graded $Cd_{1-x}Zn_xS$ Thin Films: A Route to High-Throughput Optimization for Photovoltaic Buffer Layers", Chem. Mater., vol. 25, pp. 297–306, 2013. (Article)

[36] M. Bär, A. Ennaoui, J. Klaer, T. Kropp, R. Sáez-Araoz, N. Allsop, I. Lauermann, H.-W. Schock, and M. C. Lux-Steiner "Formation of a ZnS/Zn(S,O) bilayer buffer on $CuInS_2$ thin film solar cell absorbers by chemical bath deposition", J. Appl. Phys., vol. 99, no. 12, pp. 123503-1-9, 2006. (Article)

[37] M.S. Hossain, M.A. Islam, Q. Huda, M.M. Aliyu, T. Razykov, M.M. Alam, Z.A. AlOthman, K. Sopian, N. Amin, "Growth optimization of $Zn_xCd_{1-x}S$ thin films by radio frequency magnetron co-sputtering for solar cell applications", Thin Solid Films, vol. 548, pp. 202–209, 2013. (Article)

[38] M. Birkholz, Thin Film Analysis by X-Ray Scattering, Wiley-VCH Verlag GmbH & Co. KGaA, 2006, Ch. 1. (Book Chapter)

[39] R. L. Snyder, X-ray Characterization of Materials, WILEY-VCH Verlag GmbH, 1999, Ch. 1. (Book Chapter)

[40] M. A. Islam, M. S. Hossain, M. M. Aliyu, P. Chelvanathan, Q. Huda, M. R. Karim, K. Sopian, N. Amin, "Comparison of structural and optical properties

of CdS thin films grown by CSVT, CBD and sputtering techniques", Energy Procedia, vol. 33, pp. 203–213, 2013. (Article)

[41] G. K. Williamson and W. H. Hall, "X-ray line broadening from filed aluminium and wolfram", Acta Metall., vol. 1, no. 1, pp. 22–31, 1953. (Article)

[42] G. K. Williamson and R. E. Smallman, "Dislocation densities in some annealed and cold-worked metals from measurements on the X-ray Debye-Scherrer spectrum", Philos. Mag., vol. 1, no. 1, pp. 34–46, 1956. (Article)

[43] A. R. Denton and N. W. Ashcroft, "Vegards law", Phys. Rev. A, vol. 43, no. 6, pp. 3161–3164, 1991. (Article)

[44] U. Hotje, C. Rose and M. Binnewies, "Lattice constants and molar volume in the system ZnS, ZnSe, CdS, CdSe", Solid State Sci., vol. 5, no. 9, pp. 1259–1262, 2003. (Article)

[45] J. Tauc and A. Menth, "States in the gap", J. Non. Cryst. Solids, vol. 8–10, no. C, pp. 569–585, 1972. (Article)

[46] B. E. McCandless, L. V. Moulton, and R. W. Birkmire, "Recrystallization and sulfur diffusion in $CdCl_2$-treated CdTe/CdS thin films", Prog. Photovoltaics Res. Appl., vol. 5, no. 4, pp. 249–260, 1997. (Article)

[47] S. A. Razi, N. K. Das, S. F. U Farhad, M. A. Matin, "Influence of the $CdCl_2$ Solution Concentration on the Properties of CdTe Thin Films", International Journal of Renewable Energy Research (IJRER), vol. 10, no. 2, pp. 1012-1020, 2020. (Article)

[48] L. Wenyi, C. Xun, C. Qiulong, Z. Zhibin, "Influence of growth process on the structural, optical and electrical properties of CBD-CdS films", Materials Letters, volume 59, pp. 1-5, 2005. (Article)

[49] E. Akbarnejad, Z. Ghorannevis, F. Abbasi and M. Ghoranneviss, "Investigation of annealing temperature effect on magnetron sputtered cadmium sulfide thin film properties", J. Theor. Appl. Phys., vol. 11, no. 1, pp. 45–49, 2017. (Article)

[50] O. Zelaya-Angel, L. Hernandez', O. de Melo', J. J. Alvarado-Gil, R. Lozada-Morales, C. Falcony and H. Vargas, "Band-gap shift in CdS: phase transition from cubic to hexagonal on thermal annealing", Vacuum, vol. 46, no. 8–10, pp. 1083–1085, 1995. (Article)